



## Development of a Portable Electro-mechanical Crack Monitoring Device for Pipeline Steel Materials

Oyewole ADEDIPE<sup>1</sup>, Chinedu Johnpaul MANULU<sup>1</sup>, Joseph ABUTU<sup>2</sup>, Uzoma Gregory OKORO<sup>1</sup>, Sunday Albert LAWAL<sup>1</sup>, Jonathan Yisa JIYA<sup>1</sup>

<sup>1</sup>Department of Mechanical Engineering, Federal University of Technology, Minna, Nigeria

[oye.adedipe@futminna.edu.ng](mailto:oye.adedipe@futminna.edu.ng)/[johnpaulman2010@gmail.com](mailto:johnpaulman2010@gmail.com)/[u.g.okoro@futminna.edu.ng](mailto:u.g.okoro@futminna.edu.ng)/[lawalsunday@futminna.edu.ng](mailto:lawalsunday@futminna.edu.ng)/[jiya.jonathan@futminna.edu.ng](mailto:jiya.jonathan@futminna.edu.ng)

<sup>2</sup>Department of Mechanical Engineering, Taraba State University, Jalingo, Nigeria  
[abutu.joseph@tsuuniversity.edu.ng](mailto:abutu.joseph@tsuuniversity.edu.ng)

Corresponding Author: [abutu.joseph@tsuuniversity.edu.ng](mailto:abutu.joseph@tsuuniversity.edu.ng), +2347035241729

Date Submitted: 19/02/2025

Date Accepted: 05/06/2025

Date Published 11/06/2025

**Abstract:** The pipeline infrastructure, particularly in Nigeria face significant challenges arising from defects such as cracks, which could lead to unforeseen leakage of flammable materials, risks to human and aquatic lives and could result in the loss of valuable petroleum products. This paper presents the development of a portable electromechanical device powered by lithium-ion batteries for monitoring surface pipelines for cracks, facilitating timely maintenance to prevent adverse consequences. The device is equipped with two types of electronic sensors mounted on a mobile platform that transmits data to a laptop via microcontrollers (Arduino Nano) and a USB cable. The casing of the device was constructed using polyvinyl chloride modeling board. Three tests were carried out on a 0.75 cm thick test pipe with 21 cm external diameter: No-crack test, initiated crack test, and covered crack test. Operating at 15 cm/s, the device transmitted surface condition data in real-time. The results showed no significant spikes during the no-crack and covered crack tests, while the cracked pipe test revealed spikes of 0.5 cm at positions 20 cm, 29 cm, and 38 cm along the pipe. The tractive analysis of the device indicated a net tractive force of 4.11 N and a slip value of 0.03, confirming effective movement without skidding. This study demonstrated that the developed device is reliable for pipeline monitoring and can significantly contribute to the maintenance of pipeline structures.

**Keywords:** Pipeline Monitoring, Crack Detection, Portable Device, Electromechanical Sensors, Tractive Efficiency

### 1. INTRODUCTION

Pipelines are identified as the most and fastest economical means of transporting oil and gas products, maintaining their efficiency despite fluctuations in oil prices [1-2]. Advances in technology have increased the demand for advanced pipeline grades to ensure consistent and reliable delivery of petroleum products. Pipelines offer fast, economical, and safe way to transport various products, including biofuels, natural gas, crude oil, sewage, and water over long distances [1, 3-4]. With over 1.9 million kilometres of transport pipelines globally [5-6], countries have implemented important safety regulations. Examples include Germany's Technical Rule for Pipelines (TRFL), the American Petroleum Institute (API) standards in the U.S., such as API 1130 and 49 CFR 195, and Canada's CSA Z662 standard for oil and gas pipelines.

Various leak detection methods exist for pipeline monitoring based on different working principles. These include acoustic systems, smart pigging, video monitoring, tracking dogs, helicopter inspections, fiber optic cables, sensor hoses, pressure point analysis [7-9], mass balance methods [10], statistical systems and Real Time Transient Model (RTTM) based systems. Murvay and Silea [12], Adenubi et al. [13] categorized these methods into hardware and software-based approaches, while other works [14-15] classified them into three technical categories: external, non-continuous and internal methods.

The geographical locations and vast installations of pipeline networks have enhanced the development of advanced monitoring technologies to identify cracks and leaks [16-17]. This has led to an increasing reliance on intelligent leak detection and localization systems. Ege and Coramik [16] investigated Magnetic Flux Leakage (MFL) technology through two Pipeline Inspection Gauges (PIGs), testing their effectiveness on a 5.25-meter steel pipe with artificial defects. The analysis using 2mm and 1mm-wide cracks revealed measurable peak distances (255.713 mm and 257.644 mm) in filtered sensor data that matched actual defect spacing, validating MFL's defect detection capabilities. In addition, Aguila-Munoz et al. [17] developed a portable GMR sensor-based probe for inspection of steel plate with six artificial cracks of widths 0.25- 0.5 mm and depths of 1.0-3.0 mm. The experiments showed that deeper cracks (up to 3.0 mm) produced stronger

voltage peaks and 0.5 mm cracks exhibited diminishing sensitivity beyond 1.5 mm depth. These studies have demonstrated how sensor-based technologies address pipeline integrity challenges, with MFL proving effective for linear defect mapping in pipes and GMR sensors offering precise depth assessment in controlled environments.

In addition, Aba et al. [5] proposed an IoT-based vibration-monitoring platform using pressure pulses and wireless communication via Arduino and Wi-Fi modules linked to Thing Speak. The experimental rig used five sensors to transmit real-time data, demonstrating remote damage detection capabilities. However, the study acknowledged limitations in areas with unreliable internet connectivity, highlighting a critical dependency on network infrastructure for IoT-driven systems. Also, Mazraeh et al. [18] addressed pipeline monitoring challenges by designing an ultrasonic inspection system using a Pipeline Inspection Gauge (PIG) with four symmetrically placed sensors and software-based filtering, producing a cost-effective solution for multi-diameter pipelines. The system detected an artificial crack positioned 30 cm from the pipe's edge; the work suggested that expanding sensor quantity would improve coverage for complex pipeline networks.

Most recently, Ullah et al. [19] investigated the integration of acoustic emission (AE) technology with time-series sequential deep learning algorithms for pipeline leak detection, achieving high classification accuracy in identifying leaks of varying sizes. It was recommended that incorporating this technology into smart city infrastructures would reduce environmental and economic impacts. Existing crack monitoring devices are often costly to maintain, operate manually, and they lack automation for long-distance monitoring. Hence, to address these limitations, a portable crack-monitoring device equipped with ultrasonic, infrared sensors was developed, and the performance was evaluated for pipeline inspection.

## 2. MATERIALS AND METHODS

### 2.1 Materials

The development of the device involved a range of materials categorized into tools, consumables, and mechanical and electronic components. The materials utilized included a grinding machine for creating artificial cracks, a voltammeter for measuring current flow, a soldering iron for circuit connections, a meter rule for precise measurements, an HB pencil for marking, and a retractable workshop knife for cutting purposes. Consumables comprised soldering lead and glue used for bonding device parts. The mechanical and electronic components consisted of ultrasonic and infrared sensors for distance measurement, an Arduino Nano microcontroller for data processing, a relay module for motor control, DC motors for device movement, RF transceivers for wireless data transmission, rechargeable lithium-ion batteries as the power source, a buck converter for voltage regulation, a printed circuit board (PCB) for component assembly, and a PVC modeling board serving as the device's chassis. The material used for testing was a mild steel test pipe with an external diameter of 21 cm, a thickness of 0.75 cm, and a length of 150 cm. The experimental setup included a laptop running the Arduino Integrated Development Environment (Arduino IDE) software, along with two key components: the Transmitter Unit/Inspection Device and the Receiver Unit/Controller.

### 2.2 Methods

#### 2.2.1 Design of the crack detection device

The adopted design of the crack detection device shown in Figure 1 was obtained with the aid of Catia Computer Aided Design (CAD) software.

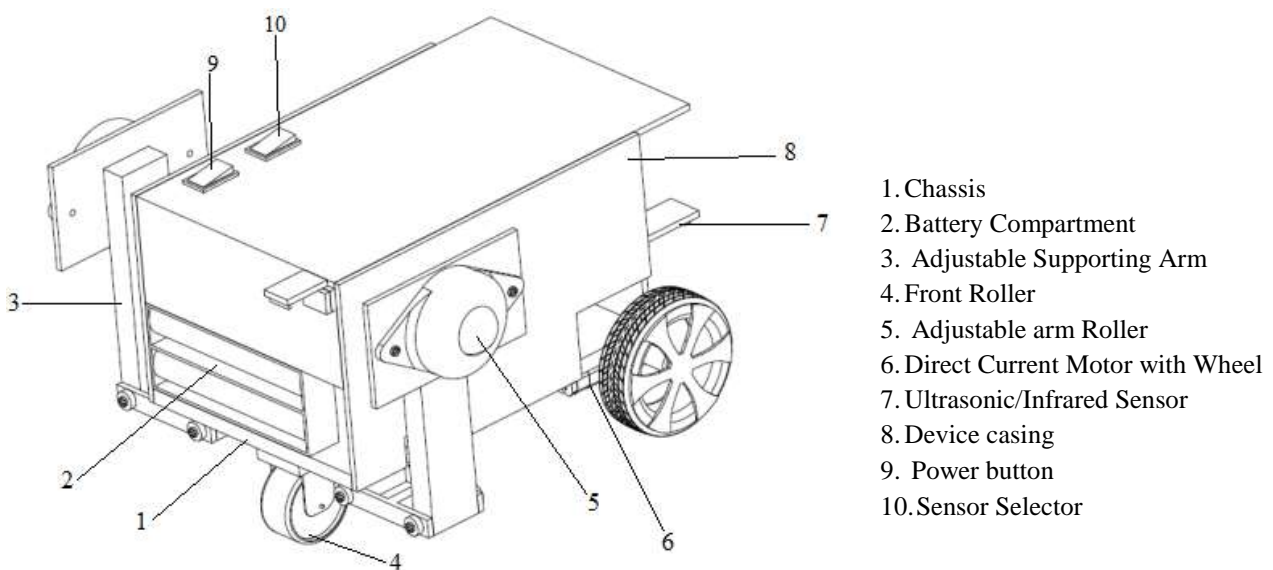


Figure 1(a): Standard isomeric view of the designed crack detection device

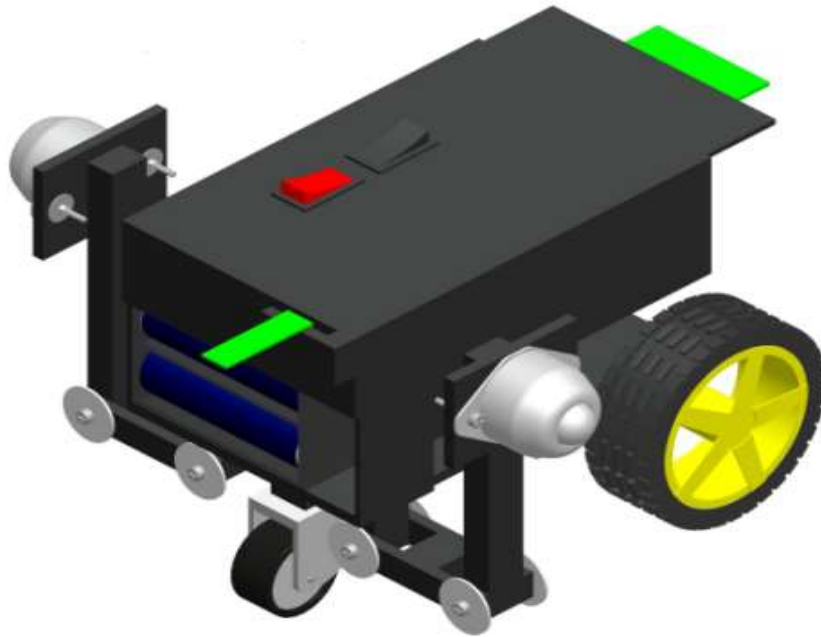


Figure 1(b): Trimetric isometric view of the designed crack detection device

## 2.2.2 Fabrication and assembly of device

### 1. Chassis

Two identical rectangular pieces of PVC modeling board, each measuring 120 mm x 85 mm x 2 mm, were bonded together using glue, resulting in a rigid board with a thickness of 4 mm, as depicted in Figure 2. Subsequently, two-wheeled DC motors were symmetrically mounted on this chassis along the wheel axis, ensuring stability and balance

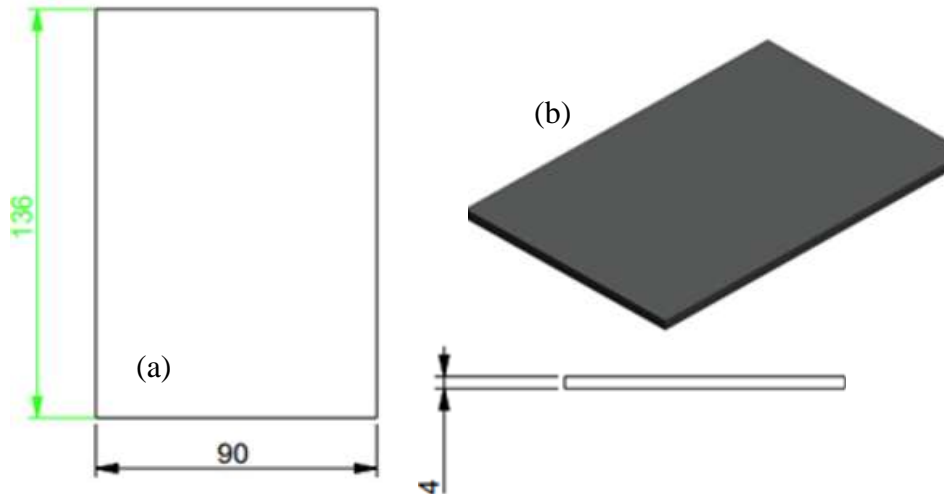


Figure 2: The chassis (a) Dimensions (b) Designed part

### 2. The adjustable supporting arm

This component, fabricated from PVC modeling board as shown in Figure 3, was attached to both sides of the chassis. The primary function was to prevent the device from slipping off the pipe surface. The component consists of adjustable bolt and nut mechanisms, allowing it to be loosened for positioning and then tightened once optimal contact with the pipe was established.

### 3. Casing

The casing (Figure 4) was constructed using PVC modeling board, known for being lightweight, durable, and easy to work with. PVC sheets were cut, glued, and shaped to form a structure suitable for model making and prototyping. The material's excellent structural properties allowed for drilling and the use of screws, making it ideal for assembling components securely. The casing, presented in Figure 4, was constructed from PVC modeling board, a material known for its light weight, durability, and ease of use. PVC sheets were cut, glued, and shaped to create a structure well-suited for model making and prototyping. The robust structural properties of the material enabled it to withstand drilling and the use of screws, making it an ideal choice for securely assembling components.

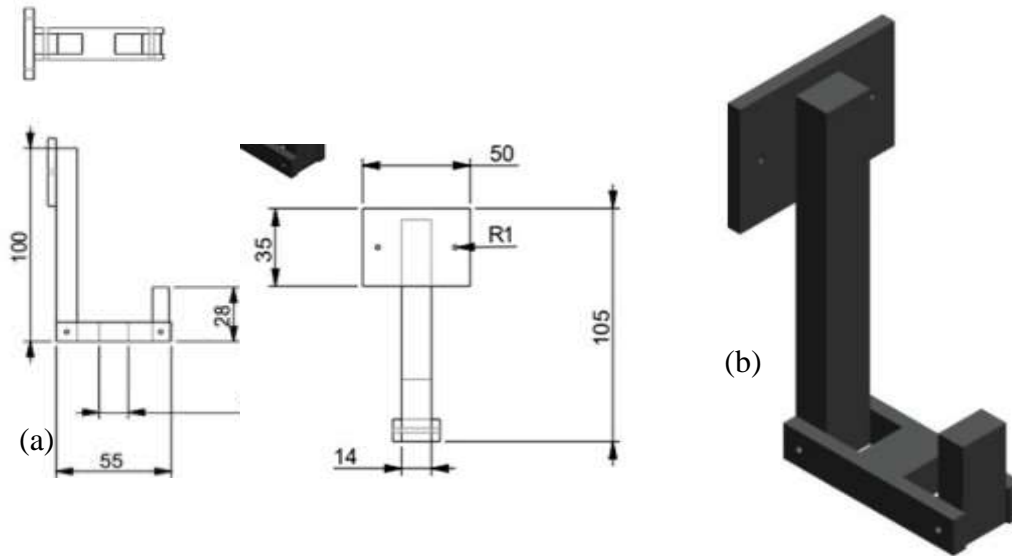


Figure 3: Adjustable supporting arm (a) Orthographic view (b) Designed part

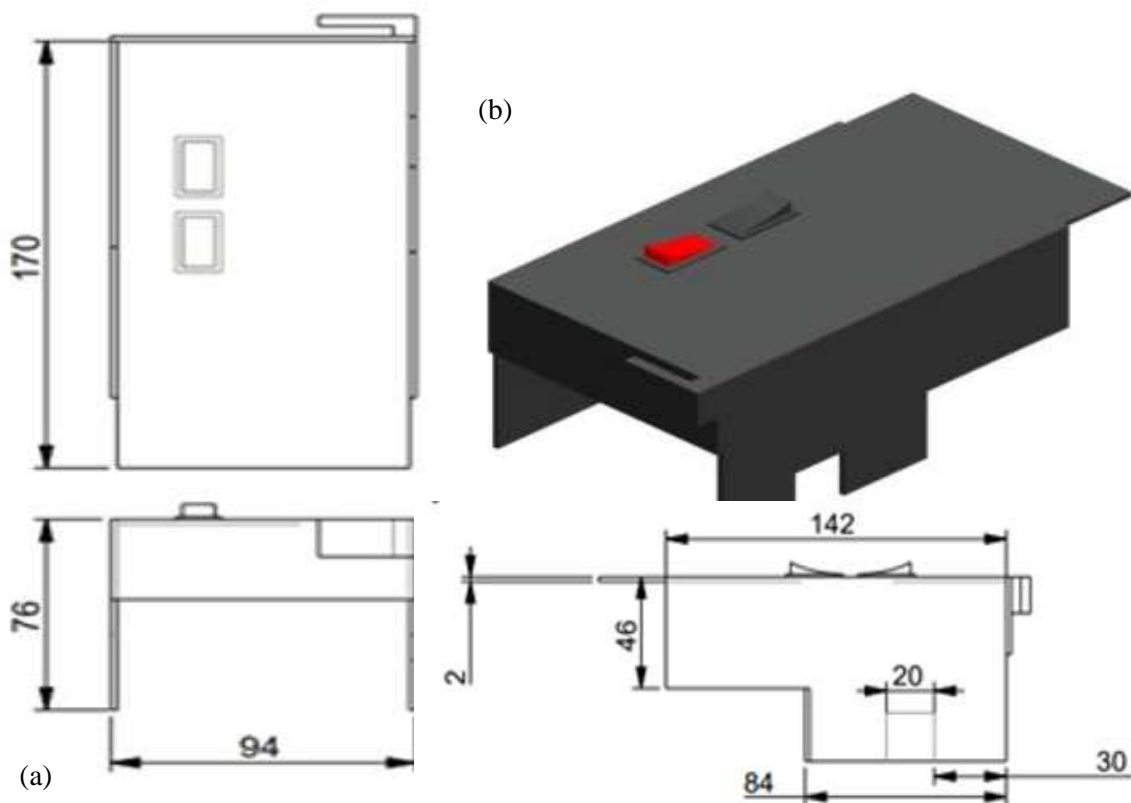


Figure 4: The casing (a) Orthographic view (b) Designed part

#### 4. The control system

The control system consists of two units: the transmitter unit, which acts as the inspection device, and the receiver unit, functioning as the controller. The transmitter unit is powered by two 3.7V lithium-ion batteries and incorporates an ultrasonic sensor, an infrared sensor, a microcontroller (Arduino Nano), a relay, a buck converter module (motor driver), and an electric motor for device movement. As illustrated in Figure 5, the Arduino Nano interfaces with both sensors and connects to the motor driver board, comprising the relay and buck converter, enabling it to send signals to regulate motor speed. While collecting data, the ultrasonic and infrared sensors relay information to the microcontroller, which then transmits it wirelessly via the radio module.

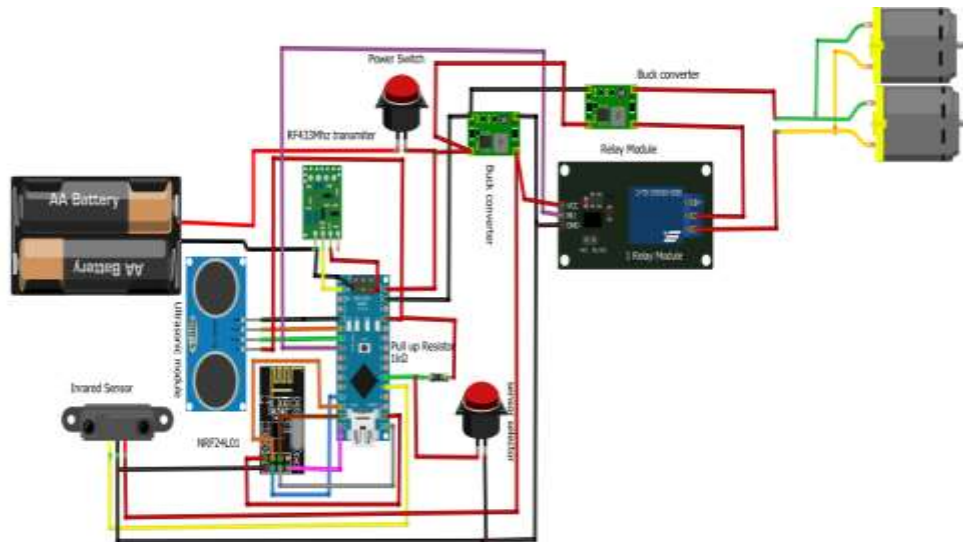


Figure 5: Circuit diagram of the developed transmitter unit

Also, the receiver unit functions as the motion controller for the device and is powered by two 3.7V lithium-ion batteries. It includes a microcontroller and a radio frequency (RF) receiver. As shown in the circuit diagram presented in Figure 6, the RF receiver is connected to the Arduino, which receives the signal and interprets it. The interpreted data was then transmitted to a computer system via the USB port

**5. Assembled device**

The assembled monitoring device, presented in Figure 7, comprises of a control system and a mobile crack detection unit. A pair of lithium-ion batteries, collectively providing 14.8V to ensure continuous operation, powers both components. The device's structural components, including the casing of the control system, the chassis of the mobile unit, the adjustable supporting arm, and the main enclosure, are all fabricated from 2 mm thick polyvinyl chloride (PVC) modeling board.

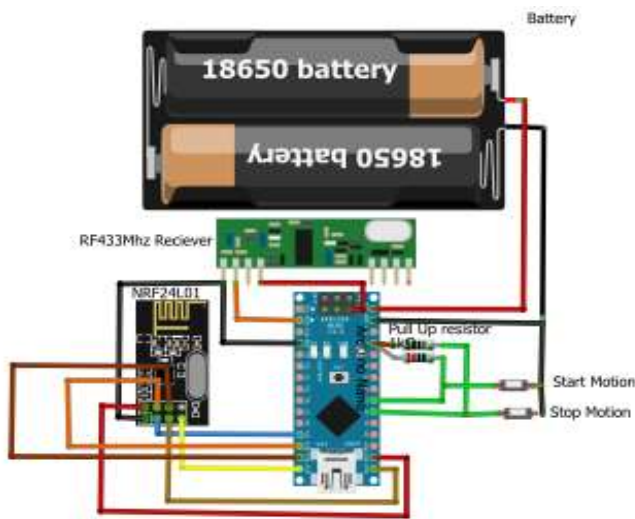


Figure 6: Circuit diagram of the receiver unit



Figure 7: Assembled device

**6. Determination of traction between the wheels and the pipe surface**

The traction devices consist of two rear wheels directly connected to the motors, while the front wheel and the wheels on the adjustable arm serve as transport devices. In the analysis, some assumptions were made: the rear wheels were simplified to a single wheel, the wheel was assumed to move at constant velocity, and the total weight of the device was considered to act on the wheel axle. This setup is shown in Figure 8, showing the forces acting at the point where the wheel contacts the pipe surface.

The parameters shown in the figure are described as presented in Equation (1-13), where  $\omega$  = Angular velocity of the wheel (rad/s),  $H$  = Net tractive force (N),  $T$  = Torque transferred to the wheel axle (Nm),  $V_a$  = Actual velocity of the wheel (m/s),  $R$  = Vertical reaction force (N),  $F_f$  = Frictional force (N) and  $W$  = Dynamic wheel load (N).

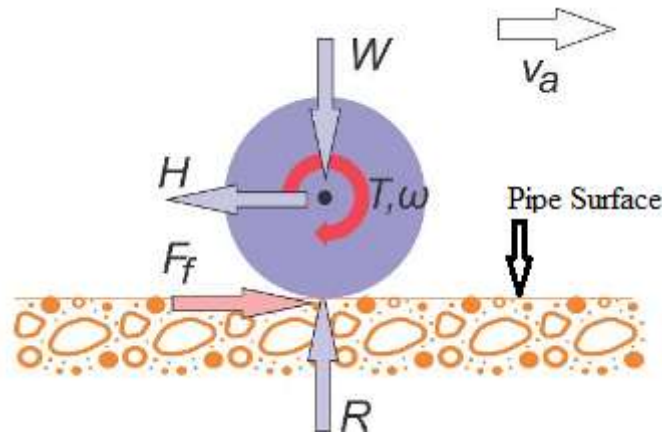


Figure 8: Wheel tractive force variables [20]

For equilibrium in the horizontal axis,

$$\sum F_x = 0 \tag{1}$$

$$H = F_f \tag{2}$$

$$\text{But } F_f \propto R \rightarrow F_f = \mu R \tag{3}$$

Where,  $\mu$  = coefficient of friction between the wheel tyre and the pipe surface

Equation (1) becomes:

$$H = \mu R \tag{4}$$

Also, for equilibrium in the vertical axis,

$$\sum F_y = 0 \tag{5}$$

$$R = W \tag{6}$$

Substituting Equation (6) into Equation (4) gives:

$$H = \mu R = \mu W \tag{7}$$

Equation (7) was used to calculate the net tractive force produced by the wheel.

The torque,  $T$  required to produce a net tractive force,  $H$  in order to overcome the frictional force,  $F_f$  is supplied by the DC motor and is transferred to the wheel axle. Therefore, the tractive efficiency of the wheel,  $T_E$  is a ratio of the tractive power,  $P_T$  and the wheel axle power,  $P_W$ . That is:

$$T_E = \frac{P_T}{P_W} \tag{8}$$

The equation for tractive power  $P_T$  is given by the product of the net tractive force  $H$  and the actual velocity  $V_a$  the vehicle or wheel [20]:

$$P_T = H V_a \tag{9}$$

$$P_W = T \omega \tag{10}$$

Therefore, Equation (8) becomes;

$$T_E = \frac{H V_a}{T \omega} \tag{11}$$

The actual velocity of the wheel,  $V_a$  is less than its theoretical value,  $V_t$  which is the velocity at which the wheel would move assuming there was no interaction between the wheel and the pipe surface.  $V_t$  is a product of the angular velocity and the radius of the wheel as given in Equation (12):

$$V_t = \omega r \tag{12}$$

A property of the wheel motion called the travel reduction ratio or slip due to the relative motion of the wheel and the pipe surface is defined as (Equation 13):

$$\text{Slip, } s = \frac{V_t - V_a}{V_t} \tag{13}$$

Slip depends on the wheel-surface conditions and varies between 0 and 1. When  $s = 1$ , the wheel does not translate rather it is rotating off the pipe surface or skidding on it. For traction to occur, slip must be greater than zero,  $s > 0$ .

**7. Determination of crack location**

The location of the crack was determined according to the relationship in [21] in Equation (14):

$$\text{Speed, } v = \frac{\text{linear distance travelled, } s \text{ (cm)}}{\text{time, } t \text{ (s)}} \tag{14}$$

From Equation (14), the location of the crack on the surface of the pipe can be deduced if the time to give a significant spike is known thus as presented in Equation (15):

$$s = vt \tag{15}$$

Equation (15) represents the location of the crack along the pipeline.

**2.2.3 Net traction between the wheels and the pipe surface**

The weight of the device is  $W = 0.6 \text{ kg} \times 9.8 \text{ m/s}^2 = 5.88 \text{ N}$  and the coefficient of friction between rubber and steel,  $\mu = 0.7$ . Therefore, the net traction force was determined using Equation (7) as:  $H = 0.7 \times 5.88 = 4.11 \text{ N}$

**1. Calculation of slip due to the relative motion of the wheel and the pipe surface:**

The time  $t$ , taken for the wheel to complete one rotation (as measured by a stopwatch) without a contacting surface is 1.41 s.

The Angular velocity of the wheel,  $\omega = \frac{\theta}{t}$

Where  $\theta =$  angular distance covered  $= 2\pi$  radians,  $\omega = \frac{2\pi}{1.41} = \frac{2 \times 3.142}{1.41} = 4.45 \text{ rad/s}$

The radius of the wheel,  $r = 3.5 \text{ cm} = 0.035 \text{ m}$ , therefore from Equation (12), the theoretical velocity of the wheel was determined as:  $V_t = 4.45 \times 0.035 = 0.155 \text{ m/s}$

The actual velocity of the wheel,  $V_a = 15 \text{ cm/s} = 0.15 \text{ m/s}$ , hence, from Equation (13), the slip was determined as:

$$s = \frac{0.155 - 0.15}{0.155} = 0.032 \approx 0.03$$

**2. Calculation of traction efficiency:**

From Equation (11), tractive efficiency is given as  $T_E = \frac{HV_a}{T\omega}$

$H = 4.11 \text{ N}; V_a = 0.15 \text{ m/s}; \omega = 4.45 \text{ rad/s}$

$T = Wr = 0.6 \times 9.8 \times 0.035 = 0.205 \text{ Nm}$

$T_E = \frac{4.11 \times 0.15}{0.205 \times 4.45} = 0.675 = 67.5\%$

**2.2.4 Performance evaluation**

The experimental setup of the developed device, as shown in Figure 9, involved positioning the inspection device on the pipe with its sensor aligned to the 0 cm start-up mark. Both the inspection device and controller unit were powered on, and the Arduino IDE software was launched on a laptop, set to the plotter option. The inspection device remained stationary until a move command was issued from the controller unit, enabling it to traverse the pipe's external surface. During testing, the plotter recorded data on the distance between the sensor and the pipe surface at the 0 cm mark over time. Subsequently, infrared and ultrasonic sensors were interchanged using their respective attachments. Upon receiving a move command, the microcontroller transmitted a signal from the transmitter to the receiver in the inspection unit, which processed it and directed the motors via the motor driver to initiate movement. A stop command could be issued at any time to prevent the device from falling off the pipe.

As the inspection device traversed the pipe, it plotted the sensor-to-surface distance against time on the Arduino IDE platform, with spikes on the plot indicating detected cracks. Operating at a speed of 15 cm/s, the device underwent three tests: first, on a crack-free pipeline to establish baseline no-defect characteristics; second, on a pipeline with three artificial cracks (each 0.5 cm deep and 1 cm wide) positioned at 20 cm, 30 cm, and 40 cm marks to simulate real defects; and finally, on cracks covered with masking tape to evaluate its effectiveness in detecting concealed cracks.

**3. RESULTS AND DISCUSSION**

**3.1 Design Calculation**

**3.1.1 Result of net traction between the wheels and the pipe surface**

The results of the calculation are given in Table 1. The net tractive force of 4.11 N indicates the effective force exerted by the wheels of the device to overcome resistance while moving along the pipe surface [22] while an angular velocity of 4.45 rad/s suggests that the wheels are rotating at a moderate speed, which is appropriate for a device designed for

inspection tasks [23]. Also, slip value of 0.032 indicates that there is minimal slippage occurring between the wheels and the pipe surface, which is desirable for maintaining traction and stability during operation. Low slip values suggest that the device can effectively translate its tractive force into forward motion, enhancing its ability to navigate along the pipe without losing contact or control [24]



Figure 9: Experimental setup

In addition, the tractive efficiency of 67.5% highlights the device's ability to effectively convert input power into useful movement. This efficiency level signifies that a substantial amount of the energy provided by the motors is being used for propulsion, rather than being dissipated as friction or other forms of resistance. High tractive efficiency is essential for optimizing battery life and ensuring sustained operation during inspections [25].

Table 1: Design calculation results

S/N	Parameter	Value
1	Net tractive force	4.11 N
2	Tractive efficiency	67.5%
3	Slip (S)	0.032
4	Angular velocity of the wheel	4.45 rad/s

### 3.2 Experimental Results

#### 3.2.1 No-crack test

The results of the no-crack test using the ultrasonic sensor and infrared (IR) sensor are shown in Figures 10 and 11, respectively. Both figures display several downward spikes, labelled as a, b, c,..., j in Figure 10 and a, b, c,..., f in Figure 11. These spikes represent a reduction in the distance between the sensors and the pipe's external surface, indicating surface irregularities or roughness at specific locations. The spikes occurred as the sensors detected bumps or imperfections on the pipe's surface, registering closer proximity [26]. This behaviour underscores the sensitivity of both ultrasonic and infrared sensors to variations in surface texture, allowing them to identify not only cracks but also other anomalies that could compromise pipeline integrity. These findings highlight the effectiveness of the inspection device in detecting structural flaws and surface irregularities, providing valuable insights into the pipe's condition.

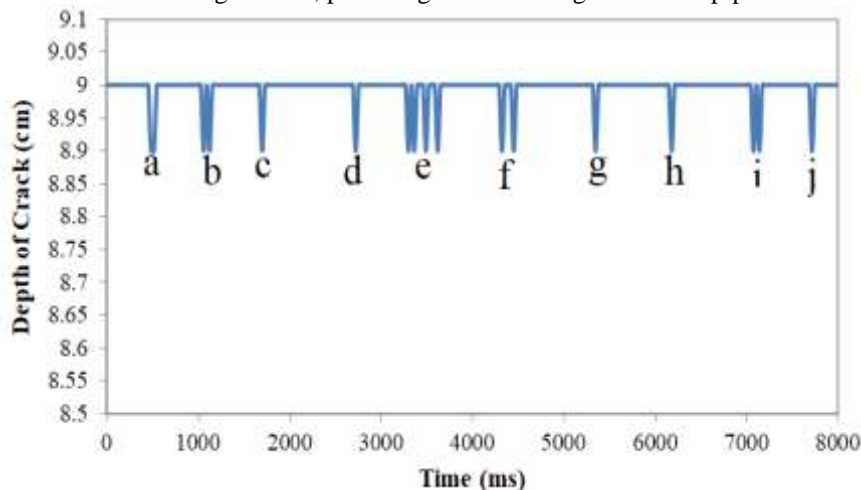


Figure 10: No-crack plot for ultrasonic sensor

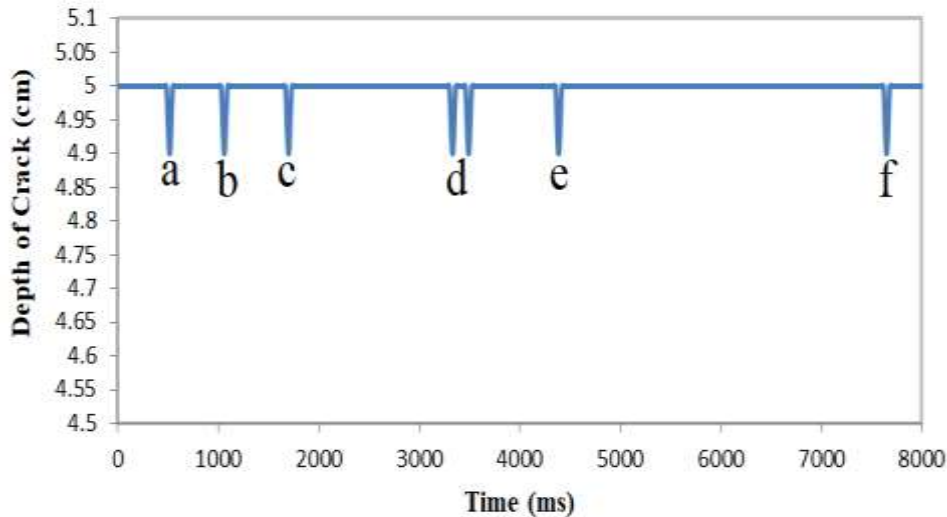


Figure 11: No-crack plot for infrared sensor

### 3.2.2 Cracked pipe test

The results of crack detectability tests using ultrasonic and infrared (IR) sensors are presented in Figures 12 and 13, respectively. Similar spikes observed in Figures 10 and 11 are also evident in Figures 12 and 13, labeled as a, b, c,..., i and a, b, c,..., f, a, b, c,..., g. These spikes represent bumps on the pipe surface with a thickness of approximately 0.1 cm at the indicated points. Additionally, distinct sharp spikes labeled A, B, and C corresponds to the positions of the initiated cracks on the pipe surface. The height of these spikes reflects the depth of the cracks, measured at 0.5 cm. Both ultrasonic and IR sensors effectively detected cracks on the pipe surface; however, the ultrasonic sensor demonstrated superior performance in identifying bumps and rough points compared to the IR sensor. This difference may arise from the roughness of the pipe surface, which reduces the amplitude of readings from the IR sensor but has minimal impact on ultrasonic sensor readings. The graphs (Figures 10 to 14) under various testing conditions highlight this distinction, emphasizing the ultrasonic sensor's robustness in detecting both surface irregularities and structural flaws.

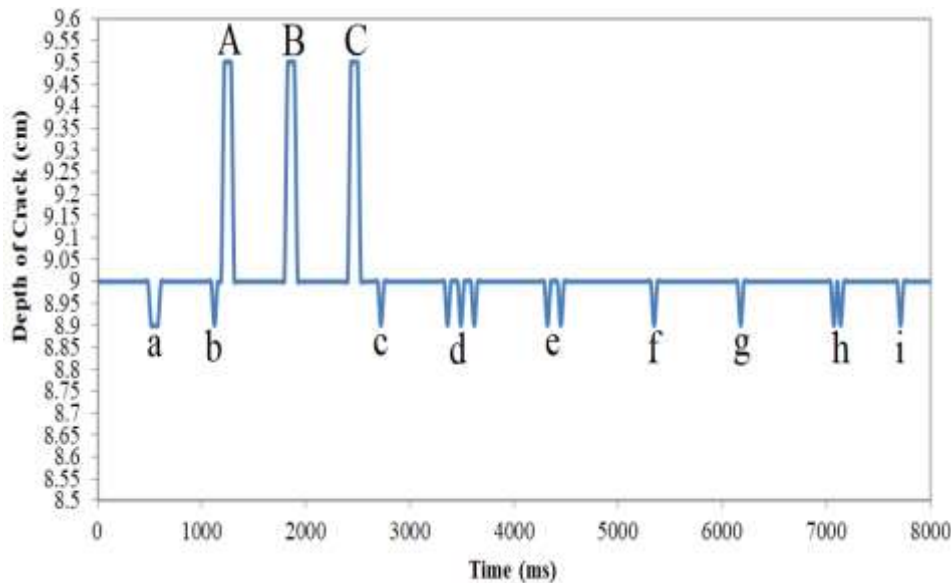


Figure 12: Cracked pipe plot for ultrasonic sensor

### 3.2.3 Covered crack test

The experimental results of testing cracks covered with masking tape, simulating the presence of foreign material on the pipe surface, are shown in Figures 14 and 15 for ultrasonic and infrared sensors, respectively. Similar to Figures 10 and 11, these figures display spikes labeled as a, b, c,..., g and a, b, c,..., f, representing bumps on the pipe surface with a thickness of approximately 0.1 cm at the indicated points. However, unlike uncovered cracks, Figures 14 and 15 exhibit mild downward spikes labeled 1, 2, and 3 at the locations of the cracks. These mild spikes suggest that the sensors as surface roughness rather than distinct cracks interpreted the masking tape covering the cracks. The masking tape's thickness was measured at approximately 0.025 cm based on the results. While the masking tape did not produce

pronounced signals like uncovered cracks, it caused slight variations in the sensor readings, demonstrating its influence on crack detection performance [27].

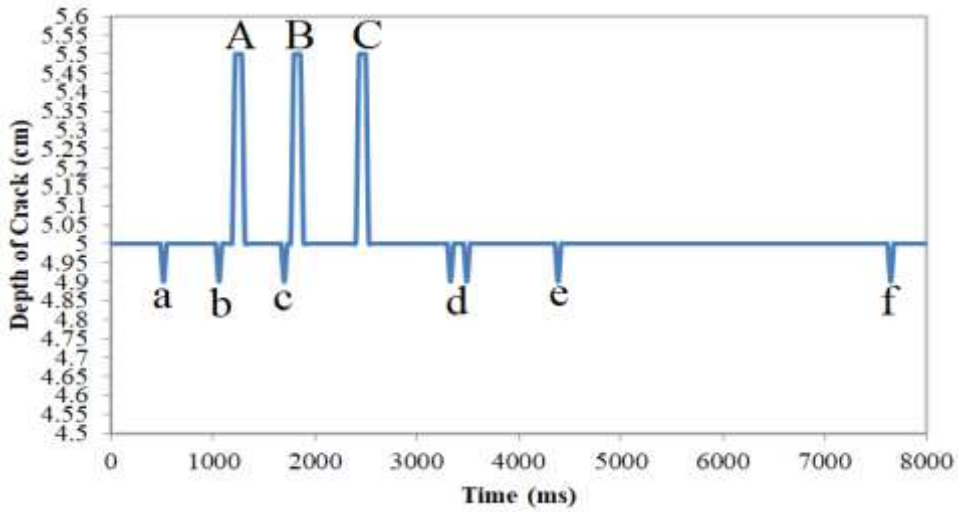


Figure 13: Cracked pipe plot for infrared sensor

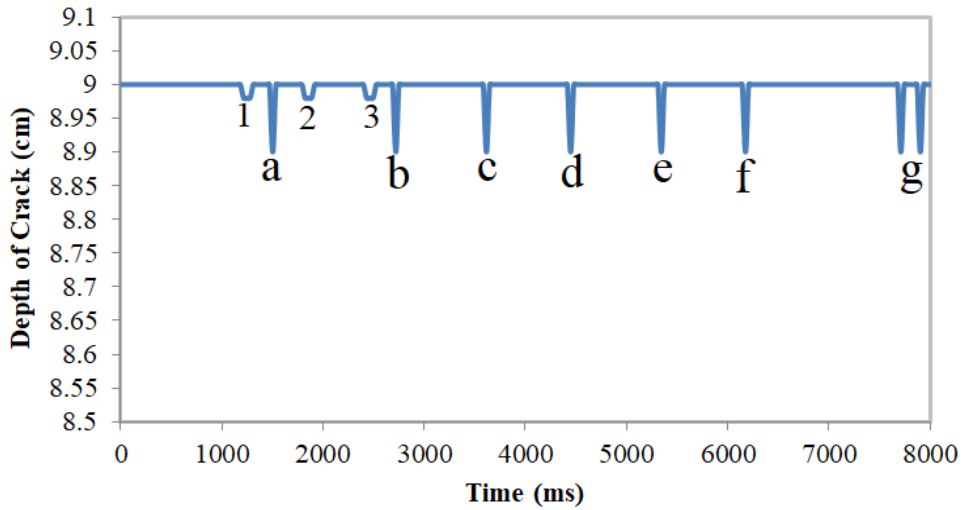


Figure 14: Covered crack plot for ultrasonic sensor

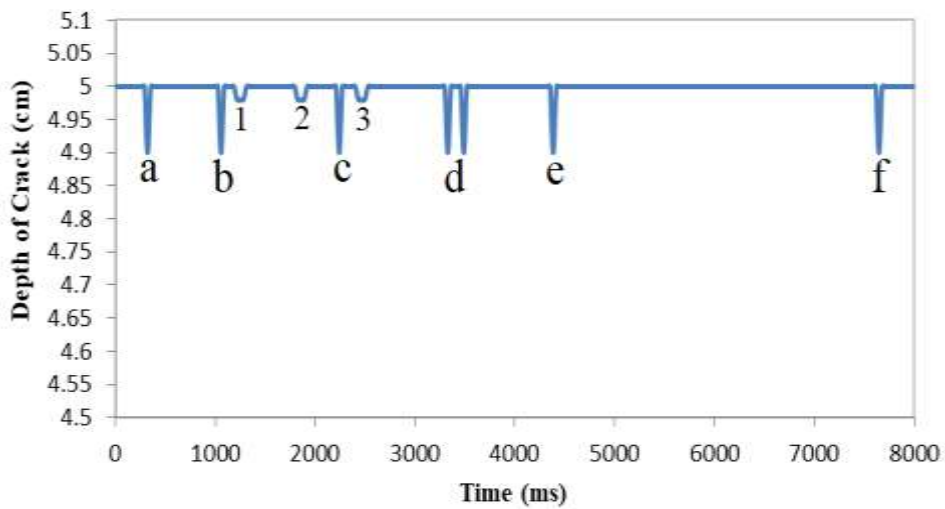


Figure 15: Covered crack plot for infrared sensor

### 3.3 Calculation of Crack Location

Location of the cracks was calculated using Equation 15 [28].

Where; the speed of the device,  $v = 15$  cm/s

From the result in Figure 12, the times corresponding to the location of the three initiated cracks are  $t_1 = 1300$  ms,  $t_2 = 1900$  ms, and  $t_3 = 2500$  ms.

Therefore, substituting into equation 15 gives:

$$s_3 = 15 \times 2.500 = 37.5 \approx 38 \text{ cm}$$

$$s_2 = 15 \times 1.900 = 28.5 \approx 29 \text{ cm}$$

$$s_1 = 15 \times 1.300 = 19.5 \approx 20 \text{ cm}$$

The locations of the three initiated cracks were determined to be approximately 20 cm, 29 cm and 38 cm respectively.

## 4. CONCLUSION

In this study, a portable crack monitoring device for pipeline structures that combines ultrasonic and infrared sensors was developed and the performance was evaluated using representative steel pipeline. The following conclusions can be drawn.

- i. The preliminary design indicated that the inspection device effectively exerted a net tractive force of 4.11 N. The device operates at an angular velocity of 4.45 rad/s, maintains a low slip value of 0.032 for optimal traction, and achieves a tractive efficiency of 67.5%. These results demonstrated its capability for efficient movement and crack detection along pipeline surfaces.
- ii. The developed device has a weight of 0.6kg and overall dimensions of 230mm x 218mm x 137mm, making it portable and easy to transport to deployment sites. It can move along the outer surface of the test pipeline without slipping.
- iii. The low-cost ultrasonic and infrared sensors showed sensitivity in detecting cracks. Graphical results revealed that crack depths were measured at 0.5 cm, matching the actual depth of the initiated cracks. Notably, the ultrasonic sensor demonstrated greater sensitivity in identifying bumps and surface roughness on the pipeline.
- iv. The device effectively detected cracks in pipelines; however, when the cracks were covered, the sensors did not register any spikes. Instead, they measured the thickness of the tape, which was found to be 0.025 cm.
- v. Overall, the findings demonstrated that the device is a reliable tool for crack detection in pipeline applications, facilitating proactive measures to address potential issues before they escalate.

## ACKNOWLEDGMENT

Authors acknowledge the support given by the Management of Federal University of Technology Minna, Nigeria for the award of Tertiary Education Trust Fund (TETFund) Institution-Based Research Intervention (IBRI) Fund (TETFUND/FUTMINNA/2024/027).

## REFERENCES

- [1] Mutiu, A. Adegboye, Wai-Keung, F. & Aditya, Karnik (2019). Recent Advances in Pipeline Monitoring and Oil Leakage Detection Technologies: Principles and Approaches. *Journal of Sensors*, 19 (11), 2548-2583.
- [2] Adedipe, O., Gambo, A. B., Abutu, J., Olugboji, O. A., Agboola, J. B., Obanimomo, K. T. & Abdulrahman, A. S. (2023). "An evaluation of mechanical properties and estimation of environmental reduction factors in welded API X70 steel pipeline in natural seawater", *Welding International*, Taylor and Francis, 37(5), 269-281
- [3] Shi, Y., Zhang, C., Li, R., Cai, M., &Jia, G. (2015) "Theory and Application of Magnetic Flux Leakage Pipeline Detection" *Journal of Sensors*, 15(12), 31036-31055.
- [4] Belvederesi, C. & Dann, M. R. (2017) "Statistical Analysis of Failure Consequences for Oil and Gas Pipelines" *International Journal of Safety and Security*, 2(7), 103–112.
- [5] Aba, E. N., Olugboji, O. A., Nasir, A., Olutoye, M. A., & Adedipe O. (2021). "Petroleum pipeline monitoring using an Internet of Things (IoT) platform", *SN Applied Sciences*,3(180), 1-12.
- [6] Fiedler, J. (2014) "An Overview of Pipeline Leak Detection Technologies" In *Proceedings of the 9th International Conference of the American School of Gas Measurement Technology (ASGMT 2014)*, Peabody, MA, USA.
- [7] Kam, S.I. (2010). Mechanistic Modeling of Pipeline Leak Detection at Fixed Inlet Rate. *Journal of Petroleum Science and Engineering*, 70(3-4), 145–156.
- [8] Tian S., Du J., Shao S., Xu H. & Tian C. (2016) "A study on a real-time leak detection method for pressurized liquid refrigerant pipeline based on pressure and flow rate" *Journal of Applied Thermal Engineering*, 95, 462–470.
- [9] He, G., Liang, Y., Li, Y., Wu, M., Sun, L., Xie, C., & Li, F. (2017) "A method for simulating the entire leaking process and calculating the liquid leakage volume of a damaged pressurized pipeline", *Journal of Hazardous Materials*, 3(32), 19–32.
- [10] Yin, S., Weng, Y., Song, Z., Cheng, B., Gu, H., Wang, H. & Yao, J. (2018). "Mass Transfer Characteristics of Pipeline Leak-Before-Break in a Nuclear Power Station" *Journal of Applied Thermal Engineering*, 142, 194–202.
- [12] Murvay, P. & Silea, I. A., (2012). A Survey on Gas Leak Detection and Localization Techniques. *Journal of Loss Prevention in the Process Industry*, 25(6), 966–973.
- [13] Adenubi, S., Appah, D., Okafor, E., & Aimikhe, V. (2023) "A Review of Leak Detection Systems for Natural Gas Pipelines and Facilities ", *Journal of Energy Technology and Policy*, 13(2), 9-19.

- [14] Boaz, L., Kaijage, S. & Sinde, R. (2014) “An overview of pipeline leak detection and location systems” In Proceedings of the 2nd Pan African International Conference on Science, Computing and Telecommunications (PACT 2014), 133-137, Arusha, Tanzania, 14–18 July 2014; IEEE: Piscataway, NJ, USA, 2014.
- [15] Cramer, R., Shaw, D., Tulalian, R., Angelo, P., & Van S. M. (2015) “Detecting and Correcting Pipeline Leaks before they become a big Problem”, Marine Technology Society Journal, 49(1), 31–46.
- [16] Ege, Y. & Coramik, M. (2018) “A new measurement system using magnetic flux leakage method in pipeline inspection” Journal of Measurement, 123, 163-174.
- [17] Aguila-Munoz, J., Espina-Hernandez, J. H., Perez-Benitez, J. A., Caleyto, F., & Hallen, J. M., (2013) “Crack Detection in Steel using a GMR-based MFL Probe with Radial Magnetization” In Proceedings of the 23rd International Conference on Electronics, Communications and Computing (CONIELE-COMP), 104-108, IEEE, March, 2013, Cholula, Mexico.
- [18] Mazraeh, A. A., Ismail, F. B., Khaksar, W., & Sahari, K. S. M. (2017) “Development of Ultrasonic Crack Detection System on Multi-Diameter PIG Robots” Procedia Computer Science, 105, 282-288.
- [19] Ullah, N., Siddique, M. F., Ullah, S., Ahmad, Z., & Kim, J. M. (2024). Pipeline Leak Detection System for a Smart City: Leveraging Acoustic Emission Sensing and Sequential Deep Learning, Smart Cities, 7(4), 2318-2338
- [20] Holden, N. M., Wolfe, M. L., Ogejo, J. A., & Cummins, E. J. (2021). Introduction to biosystems engineering. In *Introduction to Biosystems Engineering* (p. 1-570). American Society of Agricultural and Biological Engineers.
- [21] Wang, Y., Deng, H., Deng, Y., Chen, K., & He, J. (2021). Study on crack dynamic evolution and damage-fracture mechanism of rock with pre-existing cracks based on acoustic emission location. Journal of Petroleum Science and Engineering, 201, 108420
- [22] Raheman, H., & Sarkar, P. (2024). Tillage Machinery--Passive, Active and Combination. Springer
- [23] Baranidharan, M., & Singh, R. R. (2023). Solar-Powered Gearless Elevator Drive Control Using Four Quadrant DC to DC Converter System. In *Advanced Power Electronics Converters for Future Renewable Energy Systems* (83-104). CRC Press
- [24] Yan, H., Zhao, P., Xiao, C., Zhang, D., Jiao, S., Pan, H., & Wu, X. (2023, June). Design and kinematic characteristic analysis of a spiral robot for oil and gas pipeline inspections. In *Actuators*, MDPI, 12(6), 240
- [25] Gao, Y., Wu, D., Dai, Z., Wang, C., Chen, B., & Zhang, X. (2023). A comprehensive review of the current status, developments, and outlooks of heat pipe photovoltaic and photovoltaic/thermal systems. *Renewable Energy*, 207, 539-574.
- [26] Chan, K. W. (2024). Experimental Research and Failure Mechanism Detection on Temporary Flood Barrier (Master's thesis, TU Delft). Retrieved from TU Delft Repository. Mentor: D. Wüthrich
- [27] Hussain, M., Zhang, T., Jamil, I., Soomro, A. A., & Hussain, I. (2024). Application of machine learning approaches to prediction of corrosion defects in energy pipelines. *Advances in Corrosion Modelling*, 127-166
- [28] Zhang, F., Hu, Z., Yang, K., Fu, Y., Feng, Z., & Bai, M. (2021). The surface crack extraction method based on machine learning of image and quantitative feature information acquisition method, *Remote Sensing*, 13(8), 1534